Biomed Microdevices (2010) 12:821–832
DOI 10.1007/s10544-010-9436-z

Weak solvent based chip lamination and characterization of on-chip valve and pump

Peng Zhou · Lincoln Young · Zongyuan Chen

Published online: 5 June 2010

Abstract Using polystyrene as a fabrication material and pure acetonitrile as a bonding solvent, we have developed an innovative and inexpensive weak-solvent-based chip lamination process to produce highly functional, completely plastic, microfluidic chips with a 3-layer structure. This simple, scalable and rapid method allows active components, such as multiple valves and pumps, to be constructed on chip with a thin, deflectable film as the middle layer sandwiched between two polystyrene layers. Our irreversible bonding method achieves uniform lamination under mild conditions (35–45°C and 10–50 KPa) without damage to the underlying micro-features. The on-chip valve and pump structures have been systematically characterized and the pumping rate has been compared against theoretical rates predicted by mathematical modeling studies. A wide range of pumping rates (0.33–10 μL/s) can be achieved, with the integral pumps maintaining a constant pumping rate and depending on pumping frequency and pump diaphragm size. Valve leakage of less than 0.02 μL/min is noted under pressures of 41 kPa. Utilizing various configurations of on-chip valves and pumps, the fully automated flow control of an integrated chip for sample lysis, nucleic acid purification and PCR is demonstrated. The present technology and chip have been heavily evaluated internally and externally for rapid biomedical diagnosis of HPV, HIV, etc., and they are currently in the process of commercialization.

Electronic supplementary material The online version of this article (doi:10.1007/s10544-010-9436-z) contains supplementary material, which is available to authorized users.

P. Zhou (✉) · L. Young · Z. Chen
Rheonix, Inc.,
22 Thornwood Dr.,
Ithaca, NY 14850, USA
e-mail: pzhou@rheonix.com

Keywords Weak solvent · Plastic lamination · Valve and pump · Microfluidics · Lab-on-a-chip · Pneumatic

1 Introduction

Although silicon and glass substrate based chips are still in use today, the past decade has witnessed an interesting transition to glass-polymer hybrids and monolithic polymeric chips. This trend is due in part to more economical substrate and fabrication costs, unique mechanical and chemical properties, as well as the ease-of-use of disposable polymeric chips (Yager et al. 2006). In academic settings, poly(dimethylsiloxane) (PDMS), as an example, has been broadly employed to produce microfluidic chips after the Whitesides group at Harvard and the Quake group at Stanford successfully developed soft-lithography technology (McDonald et al. 2000), and pneumatically-actuated valves and pumps (Unger et al. 2000), respectively. Thermoplastic materials such as polycarbonate (Chen et al. 2007; Liu et al. 2004a), poly(methyl methacrylate) (PMMA) (Martynova et al. 1997; Brown et al. 2006; Shah et al. 2006; Tsao et al. 2007) and cyclic olefin polymer (COC) (Steigert et al. 2007; Zou et al. 2007; Shinohara et al. 2008; Mair et al. 2007) have also been frequently used as chip substrates. As Whitesides (2006) pointed out, however, it is not apparent whether PDMS or one of engineered plastics will ultimately dominate as the microfludic chip substrate material of choice.

A microfluidic chip capable of multiple on-chip functions requires a complicated fluid flow control that can be achieved by the proper use of on-chip valves and pumps. Although considerable effort has been devoted to the development of microvalves, many are miniaturized versions of conventional macrovalves. Some have been based

on novel concepts such as elastomer (Unger et al. 2000; Go and Shoji 2004; Gu et al. 2007), hydrogel (Beebe et al. 2000; Luo et al. 2003; Baldi et al. 2003; Wang et al. 2005), paraffin (Pal et al. 2004; Liu et al. 2004b; Hua et al. 2008), and ice valves (He et al. 2001; Chen et al. 2005). While these innovative valves provide many advantages, some of them also suffer from several significant shortcomings such as biocompatibility concerns, fabrication difficulty, operation challenge, and/or relatively slow response.

In addition to valves, pumps represent another key component for the control of microfluidic flow. While most groups continue to rely upon external pumps to drive the fluid flow within chips, a few groups have developed their own integrated on-chip pumps, which promise more flexible fluid flow manipulations. Moreover, such onboard pumps offer the possibility of significantly reduced cost devices since expensive external micropumps would be unnecessary. There are several distinct mechanisms to achieve on-chip pumping. Conventional approaches include peristaltic (McDonald et al. 2000; Gu et al. 2007) and diaphragm-based (Grover et al. 2003) actuation. More unconventional approaches include various kinds of driving mechanisms based on fluidic body forces induced by electroosmotic (Zeng et al. 2001; Brask et al. 2005), magnetic (Hatch et al. 2001; Pipper et al. 2007) or magnetohydrodynamic (MHD) effects (Lemoff and Lee 2000; Bau et al. 2003). Peristaltic pumps stand out as an excellent candidate, based upon their reliability, reproducibility, and compatibility with bioprocesses and fabrication along with their demonstrated successful use in many complex microfluidic control applications.

Conventional lamination technologies for plastic chips involve either thermal bonding or solvent based bonding. Thermal bonding around the glass transition temperature of thermoplastic materials such as polycarbonate and acrylic is often achieved at the expense of deformation of the micro component's features (Tsao et al. 2007). To reduce the thermal deformation, several groups have recently reported their achievements with thermal bonding at temperatures lower than glass transition temperatures after pretreating the bonding surfaces with oxygen plasma (Shinohara et al. 2008) or UV/O_3 (Tsao et al. 2007). Additionally, thermal bonding requires long cycle times, varying from minutes to hours.

While conventional solvent-based bonding offers no such thermal deformations, it nevertheless often leads to channel surface roughening, leakage due to incomplete bonding, as well as loss or blocking of fine features due to an excess of strong solvent allowed to remain in the channel for periods longer than 2-3 s. (Shah et al. 2006). Recent developments on solvent vapor based or solvent aided bonding are encouraging. Mair et al. (2007) reported cyclohexane vapor based bonding at room temperature that requires a prescribed amount of time and a subsequent exposure of the bonded chip to UV light to strengthen the bond between mating parts.

Wallow et al. (2007) took advantage of the permeation boundary of case-II diffusion by immersing the lid coupon and dipping the pattern coupon in an ethanol-decalin mixture to achieve a bond at temperatures 30°C lower than that required by conventional thermal bonding. This method requires a good understanding and control of multiple factors including permeant composition, permeation depth, bonding temperature, bonding pressure, and ancillary rinse and drying steps.

To sum up, the most successful fabrication method is oxygen plasma or UV/Ozone based bonding of elastic material-PDMS slab/film. To take advantage of thermoplastic material availability, low cost and good mechanical, thermal and chemical properties, there has been strong pressure to develop plastic based microfluidic devices. To our knowledge, there is sparse reporting of plastic film bonding aimed at fabrication of microfluidic devices with complicated flow control. Traditional solvent bonding simply can not meet the requirements such as no damage to fine design features, uniform and complete bonding over contact surfaces, fast process, simple operation, low cost, high yield, etc. To address the shortcomings discussed above, we present a unique design and novel fabrication technology for rapidly producing (within a few seconds) multiple valves and pumps in a chip at an economical cost. Our disposable chips are constructed from polystyrene (PS), an engineered thermoplastic polymer. Using our own weak solvent based bonding technology (Zhou and Young 2009), we have been able to fabricate chips by sandwiching one thin PS film between two thicker PS layers. Our chip design features microfluidic channels on one PS layer and circular chambers used for pneumatic control on the other PS layer. Once bonded, these three PS layers form a diaphragm-based actuation structure. Our lamination process provides an easy way to manufacture multiple components such as valves, pumps, and reaction chambers within the microfluidic device (Young and Zhou 2006). We present a detailed description of our design and fabrication methodology, followed by substantial characterization data. Finally, we present and discuss a number of microfluidic components for typical operations including fluid transport, mixing, routing and sealing that result from our lamination process.

2 Weak solvent based lamination without damage to micro features

Solvent lamination, or solvent welding, often refers to the practice of joining two or more discrete plastic parts by

treating the joint with an organic solvent to form an irreversible bond. Common organic reagents used for solvent lamination include acetone, chloroform, methylene chloride, methylethyl ketone, tetrahydrofurane and various other aromatic molecules. These agents may also be mixed together with a small amount of dissolved polymeric material in order to achieve a strong bond with the desired characteristics (i.e., bond time, gap filling ability, etc.). Although solvent lamination has been previously mentioned in the literature (Shah et al. 2006; Mair et al. 2007; Wallow et al. 2007) as a potentially useful method for fabricating polymeric microfluidic chips, to our knowledge, it has not been widely practiced in the field. This is primarily due to the fact that all of the known solvents tend to damage or completely destroy the fine structures required to produce a microfluidic network.

Despite this issue, we have learned that pure acetonitrile can be used to laminate polystyrene substrates, with excellent bonding characteristics, without ensuing damage to the micro-features. The most striking fact of the polystyrene/acetonitrile lamination system is that the irreversible bond forms under mild temperature (35–45° C) and pressure (10–50 KPa) within a few seconds. On the other hand, if the lamination is attempted at room temperature, the opposing surfaces remain unattached. Although it is well known that the solubility of most inorganic or organic substances increases as the temperature rises, utilizing this solubility variation for controlled microfluidic structure solvent lamination requires a narrow operating window. The remarkably large variation in the solubility strength of acetonitrile at different temperatures, when used in relation to polystyrene, makes it ideal for microfluidic chip fabrication. Figure 1 shows that when a test coupon containing fine features (2.5–3.5 μm) was treated in pure acetonitrile for several minutes, no structural changes were observed. Since acetonitrile is minimally aggressive to the polystyrene surface, we refer to this lamination process as "weak solvent lamination".

2.1 Valve and pump mechanism

3-layer active component structure The basic component of a valve or pump is 3-layer active component structure (Fig. 2): a top layer, a bottom layer and a thin film sandwiched between them. The upper layer contains milled microfluidic channels. The corresponding bottom layer contains diaphragm pockets, and apertures within the pockets to permit communication with the driving pneumatic signal provided by the controller. The completed structure contains a deflectable diaphragm structure covering the two ends of the disconnected channels. The dimensions of the valve pocket, aperture diameter and channels are typically 2-10 mm, 1 mm and 0.2–0.5 (depth) x 0.3–1.0 (width) mm, respectively.

Valve mechanism Shown in Figure 3(a), when positive pressure is applied to the diaphragm, normal to the top substrate, the diaphragm is pushed upwards toward the top substrate, effectively closing the fluidic communication between the two channels. We refer to this as the "Valve Closed" position. Similarly, if the diaphragm is pulled away from the top substrate by negative pressure, the diaphragm deforms into the pocket in the bottom substrate, resulting in fluid flow from one channel to the next. By allowing the connection of two discontinuous channels, we have effectively achieved a "Valve Open" position.

Pump mechanism As shown in Fig. 3(a), when the diaphragm is pulled away from its relaxed position to deform into the diaphragm pocket, an enclosed volume is

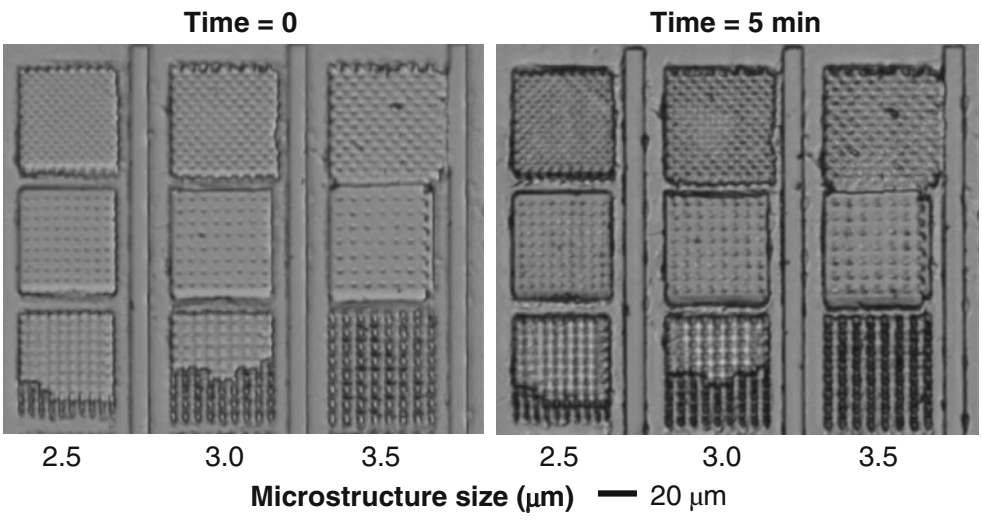

Fig. 1 Image of the test microstructures before and after exposure to pure acetonitrile. Test microstructures ranging from about 2.5 to 3.5 μm in size, and approximately 10 μm in depth were replicated on 1 mm thick polystyrene sheets. Time = 0 and Time = 5 min are images taken prior to and after a 5 min acetonitrile treatment at room temperature

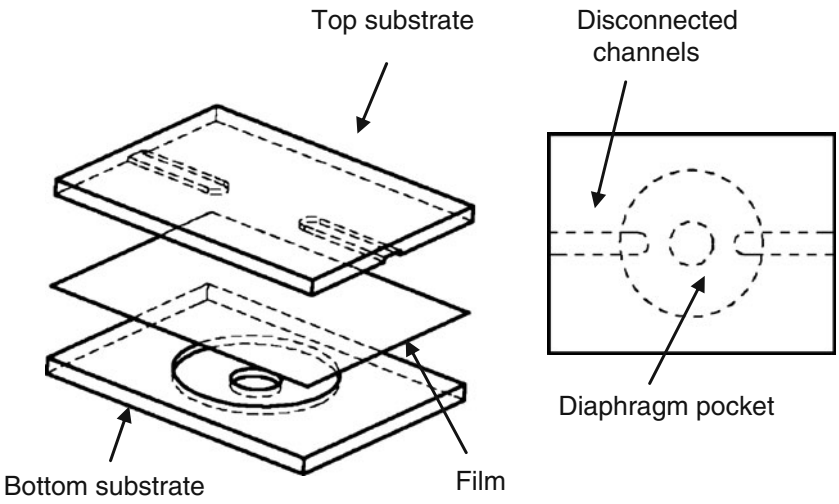

Fig. 2 The exploded perspective and top view of the 3-layer chip structure. The disconnected channels, diaphragm pocket and aperture for conduction of pneumatic signal, a deflectable film, are solvent laminated to form an on-chip active fluid control component

created. Not only does this enclosed volume allow fluid communication between the disconnected channels, but it also causes some of the fluid in the channels to move into the displaced volume. This transfer of fluid makes it possible to form a pump by continuously actuating multiple diaphragms placed in series, by sequential positive and negative pressure, interconnected by disconnected channels, as shown in Fig. 3(b). Reversing the actuation sequence of the first and last valve diaphragm changes the fluid flow direction, thus the pump is bi-directional. The duration of one pumping cycle is typically 1 s. The size of pumping diaphragm can be designed to achieve the desired pumping capacity and strength, depending upon the specific application. The diaphragm size typically ranges from 4 to 8 mm. The video "Pumping Animation" is available in the Supplementary Material.

2.2 Materials and fabrication

We used polystyrene (PS) as the substrate, with the top and bottom layers composed of 1 mm thick PS (Plaskolite, Columbus, OH). The intervening thin PS film (Trycite, Dow) has a thickness of 25 μm. Both the thick and thin PS materials are a common product and were used as obtained from the manufacturer. We selected PS as the chip substrate because of its dimensional stability (relatively unaffected by temperatures up to 90°C), excellent mechanical strength

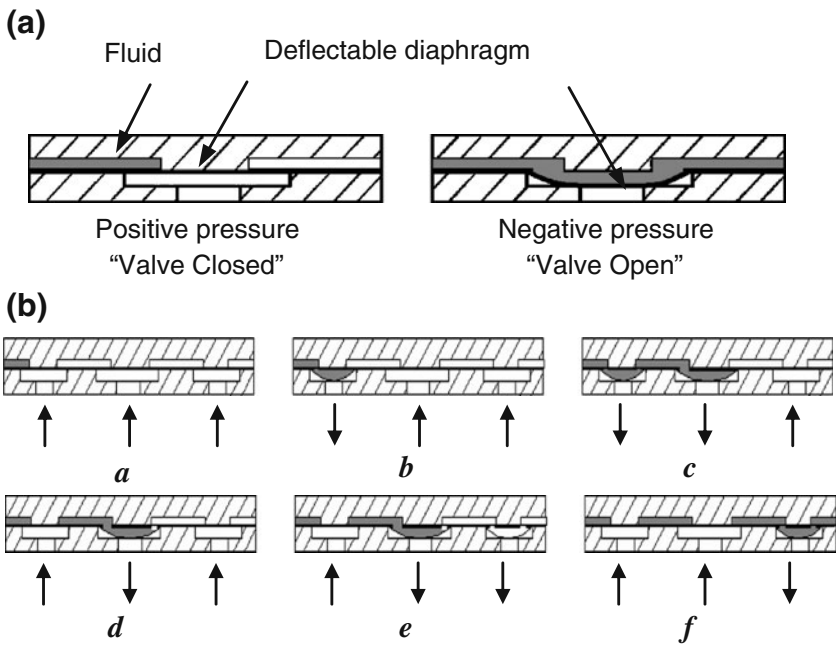

Fig. 3 Cross-sectional view of the on-chip valve and pump. (**a**) Valve closed and open position. (**b**) A pumping cycle consists of six pump states, a-f, to move fluid from the inlet channel to the outlet channel. Arrows indicate the pneumatic force applied to the diaphragm. Before starting, the pump is in state a, all valves are closed. In state b, the inlet valve is opened and fluid is drawn from inlet channel to the inlet valve. Next in state c, the pump valve is opened, drawing more fluid into the pump system. In state d, e and f, the inlet valve is closed, the outlet valve is opened and pump diaphragm is closed respectively

and stiffness. More specifically, its Young's Modulus (3–3.5 GPa), on one hand, is relatively high among plastic materials and therefore is especially good for structure formation via either machining or injection modeling. On the other hand, it is much lower than those of inorganic and metal materials (e.g., glass, aluminum in the range of tens GPa), providing an acceptable elastic region for film based diaphragm actuation. Moreover, PS is well known for its sanitary quality and wide applications in bioresearch and science (e.g., Petri dishes, test tubes) and food package industry.

The various chip designs were laid out using SolidWorks CAD software (Concord, MA). The fabrication process starts with the machining of the chip parts, followed by our weak solvent process to laminate those parts into the final chip. A computer numeric control (CNC) mill (HASS OM-2A), suitable for prototyping work, was used to machine the chip parts. Injection molding or hot embossing will be used for our future mass production for commercialization.

The chip lamination process is schematically described in Fig. 4. It starts by first dispensing pure acetonitrile, in a controlled manner, between the thin polystyrene film and the bottom polystyrene substrate, followed by rolling the solvent impregnated interface through a hot-roll laminator (DF-4200 14"Think & Tinker, Ltd., Palmer Lake, CO) at a temperature of about 40°C. Any excess solvent remaining inside of the diaphragm is quickly removed by either vacuum or by blowing compressed air across the parts. Once completed, the top substrate, which contains the microfluidic channel features, is then same solvent laminated to this pre-bonded, polystyrene film–substrate on an in-house developed hot press at 35°C and 10–50 KPa within 8-9 s. In order to form active, functional on-chip components such as valves or pumps, it is critically important to prevent the deformable film from bonding to the top substrate in the diaphragm pocket area. We accomplish this by using negative pressure during the second bonding step to deflect the film away from the top substrate. Furthermore, lamination with more than three layers can also be readily performed to achieve a three-dimensional microfluidic network.

2.3 Bonding method comparison and mechanisms

Compared to the two-step method developed by US Sandia National Laboratories (Wallow et al. 2007), our single-step bonding method offers significant advantages with respect to process time and simplicity. Wallow's method is to pretreat test coupons in a decalin: ethanol mixture (80:20 w/w) for 15 min (lid coupon) and 30 s (patterned coupon) at room temperature (first step). After rinsing and drying, the two coupons are mated and inserted into a hot press followed by 15 min heating up to 60°C without pressure applied, 20 min held at 180 psi, 10 min cooling down to less than 27°C (second step). This bonding method is interpreted by the authors as swelling by the permeant via case II diffusion which allows increased polymer chain movement, that in turn results in greater plasticity and a decreased glass transition temperature in the permeated layer.

More recently, Ng et al. (2008) reported isopropanol (IPA) aided thermal bonding of PMMA (T_g 100°C) at 70°C for 10–15 min. Similarly, no bonding occurs at room temperature. They explained this phenomenon with a different mechanism. At lower temperatures, PMMA is not soluble in IPA. But as temperature increases, it gets

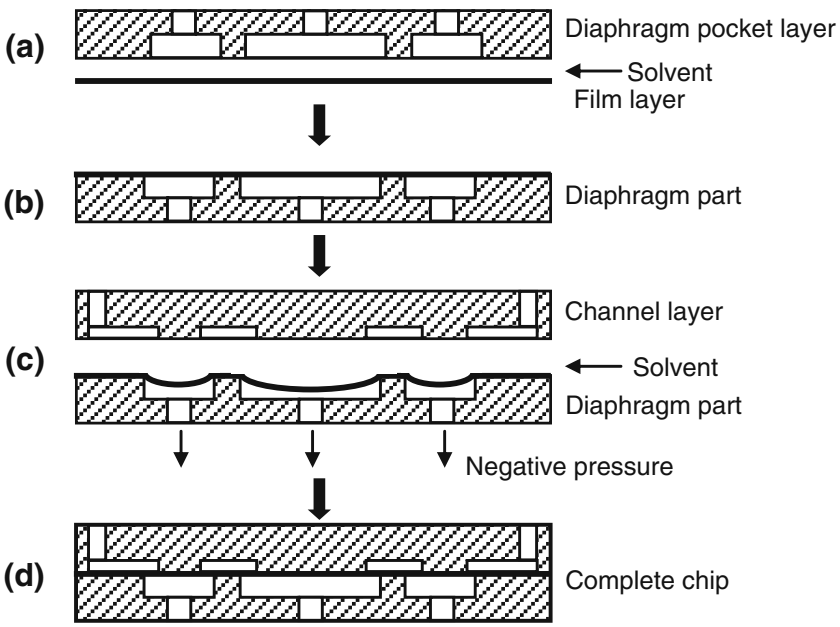

Fig. 4 Schematic description of chip lamination. (**a**) apply solvent to the film, place diaphragm pocket layer atop, and roll the assembly through a hot-roll laminator at 40°C; (**b**) complete diaphragm part; (**c**) apply solvent to the diaphragm part, place the channel layer atop, deflect diaphragms with negative pressure, and laminate on a hot press at 35°C; and (**d**) complete chip

more and more soluble as their solubility parameters approach each other's. The mechanism for solvent based lamination is to dissolve the polymer from the opposite bonding surfaces with the solvent to facilitate the inter-diffusion of polymer chains. The dissolution of polymer is based on one of the *basic principles* of chemistry, "*like dissolves like*". The Hildebrand solubility parameters, $\delta = (\Delta E_v/V)^{1/2}$, in $(MJ/m^3)^{1/2}$ and $\Delta E_v = \Delta H_v - RT$, where ΔE_v is the energy of evaporation, V is the molar volume, ΔH_v is the molar heat of vaporization, and R is the gas constant. When following this mechanism, however, we have difficulty interpreting our acetonitrile based PS bonding. At room temperature, the solubility parameters of acetonitrile and PS are 24.1 and 18.0, respectively and therefore acetonitrile at room temperature is not a solvent to PS due to the big difference in their solubility parameters. At the bonding temperature of 45°C, acetonitrile's ΔH_v = 33,040 J/mol and its solubility parameter is calculated to be 23.3 (Green and Perry 2008). The solubility parameter of PS at 45°C is estimated to be 18.3 following a model $\delta = \delta_g + m_s (T–T_g)$, where m_s = -0.0166 $(MJ/m^3)^{1/2}$ /K, T_g = 100+273.15 = 373.15 K, δ_g = 17.38 (Chee 2005). Accordingly, the difference in solubility parameters between acetonitrile and PS is not significantly decreased at higher temperature and this hardly explains why the bonding can be achieved at 45°C.

Therefore, we propose a thermally-enhanced case II diffusion mechanism aimed at better interpretation of our bonding. Since in our single-step bonding method both solvent and plastic substrates are subject to mild temperature (35–45°C) and pressure (10–50 KPa), the effect of temperature on case II diffusion needs to be addressed. Case II diffusion, i.e., relaxation controlled absorption kinetics appears as Arrhenius behavior although the process does not involve a chemical reaction (Hopfenberg et al. 1976). The case II diffusion rate constant, $k = Ae^{-E_a/RT}$, where A is the pre-exponential factor, R is the gas constant, T is temperature, and E_a is activation energy. Both activation energy E_a and the rate constant k are experimentally determined and represent macroscopic diffusion-specific parameters which are not simply related to threshold energies; and E_a is assumed independent of temperature for convenience and simplicity. Thermodynamic analysis, however, shows that E_a (related to Gibbs free energy) is a function of temperature. We believe the increase in temperature would result in E_a decrease, which together with the contribution of temperature change itself in the rate constant equation would lead to a higher rate constant. This enhanced case II diffusion due to increase in temperature would significantly speed up the relaxation and swelling of opposite surfaces resulting in a much faster bonding (in our case within a few seconds).

3 Characterization

Characterization of the valve and pump has been extensively conducted to gain a better understanding of the performance of present designs under various operating conditions and to assist future design revisions if necessary. The following characterization work was conducted using water as a flow fluid unless indicated otherwise.

3.1 Valve

The sealing capability of the valves was evaluated (setup and data charts presented in Supplementary Material Fig. S1–S3). We have found that the quality of the sealing is strongly correlated to the fabrication process. Under relatively high backpressure (i.e., 55 kPa), out of a total of 60 valves evaluated, 45 valves showed leakage of less than 0.2 μL/min, while an additional 7 valves showed leakage of less than 0.3 μL/min. Note that these tests were carried out with pneumatic sealing pressure applied to the valve diaphragm held constant at 96 kPa.

The effect of backpressure on valve leakage was further investigated by varying the backpressure in the liquid from 14 to 69 kPa with the pneumatic sealing pressure maintained at 96 kPa. A chip with four low leakage valves was chosen for this investigation. At backpressures of 14, 28, 41 kPa, the average leakage rates are 0.003, 0.009 and 0.02 μL/min, respectively. The leakage became serious as the applied pressure neared 41 kPa. Fortunately, most on-chip operations can be carried out with relatively low backpressures (< 41 kPa). Our recent improvement in lamination quality significantly increases valve sealing capability (data not shown here).

Another investigation was conducted to examine the effect of sealing pressure (pneumatic pressure applied to the valve diaphragm) on valve leakage. For this case, the backpressure of the liquid was maintained at 55 kPa while the sealing pressure was increased from 52 to 110 kPa. At a sealing pressure of 52 kPa, the average leakage rate is greater than 1 μL/min. Clearly, the turning point of the curve is at a sealing pressure of approximately 55 kPa, which is equal to the backpressure of the fluid. As noted, there is no significant improvement in prevention of leakage at sealing pressures greater than 69 kPa. These results serve as a guide to setting the pressure for valve control.

3.2 Pump

The pump was also characterized in terms of stroke, diaphragm size, positive pressure, negative pressure, backpressure, pumping frequency, and reproducibility (detailed setup and data charts presented in Supplementary Material

Fig. S4–S9). A stroke is referred to as one complete pumping cycle. Pumping capacity is defined as the pumped volume per stroke (μL/stroke), while pumping rate is defined as pumping volume per second (μL/s).

3.2.1 Accumulated pumping volume: as a function of stroke number

It was expected that the accumulated pumping volume would be proportional to stroke number. This test was done with 5.3 mm and 4.7 mm diaphragms. Both R-squared values of the fitting lines close to 1 indicate an excellent linear relationship between the pumping volume and the number of pump strokes and thus confirm stable pumping rates. The pumping capacity of the 5.3 mm and 4.7 mm diaphragms can be determined from the slope of the individual lines, i.e., 1.35 μL/stroke and 0.87 μL/stroke, respectively.

3.2.2 Pumping capacity: as a function of diaphragm size

Four pumping diaphragms of different diameters (4.7, 5.3, 6.3 and 8.5 mm) were evaluated using a positive and negative drive pressure of 60 kPa and –55 kPa, respectively. It is not unexpected that an exponentially increasing pumping capacity curve was regressed from measured data in Fig. 5. The regressed pumping capacity (F, μL/stroke) is a function of diaphragm diameter (d, mm) only if other operation parameters remain unchanged.

$$F = 0.0061\ d^{3.23} \tag{1}$$

In general, the pumping capacity should be directly proportional to the deflection volume of the pump diaphragm. However, other factors may influence the relationship between deflection volume and pumping volume. Such factors include pumping frequency, the quality of the valving and the flow resistance of the channels. To determine the efficiency of the pumps, a series of deflection volumes were measured with dyed water using pumps with different diameters (triangle points shown in Fig. 5). The fitted curve of the deflection volume is higher than that of the pumping capacity. The difference between these two curves becomes more apparent as the diaphragm diameter increases, suggesting a loss of pumping efficiency. The regressed equation for this deflection volume (V, μL) vs. diameter (d, mm) is

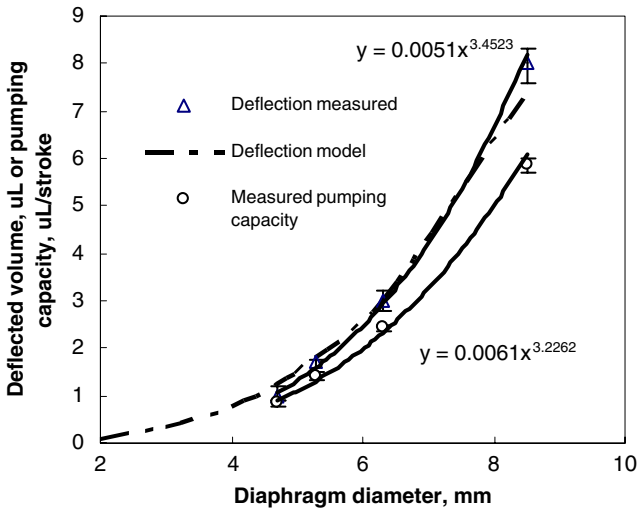

Fig. 5 Pumping capacity and deflected volume as a function of diaphragm size

$$V = 0.0051\ d^{3.45} \tag{2}$$

Modeling of diaphragm deflection. To model the diaphragm deflections, several assumptions can be made: 1) the deflection is dome shaped; and 2) the height of dome (h, mm) is linearly related to the diameter (d, mm) of the base of the dome, e.g., the diaphragm diameter. The linear relationship is $h = 0.0305d$ based on measurements of deflection at a negative pressure of 55 kPa. Accordingly, the dome's radius (r_c, mm) of curvature is expressed as

$$r_c = \frac{h^2 + (d/2)^2}{2h} = 4.1136d \tag{3}$$

Therefore, the volume of the dome or the deflection volume (V, μL) is

$$V = \pi r_c h^2 - \frac{1}{3}\pi h^3 = 0.012d^3 \tag{4}$$

Equation 4 is depicted in Fig. 5 as a dashed line that is very close to the measured deflection volume curve. The above regressed equations and the modeled equation can be used as a guide to pump design and improvement. Our recent design of smaller size of pumping diaphragm (diameter 3.5 mm) provides a pumping capacity of 0.33 μL/stroke, very close to 0.35 μL/stroke calculated from Eq. 1.

3.2.3 Effects of positive pressure, negative pressure and backpressure on pumping capacity

It was expected that the pumping capacity would not be dependent on the positive pressure applied to the diaphragm. The negative pressure was maintained at –55 kPa. Positive pressure forces the deflected diaphragm back to a flat position, thus driving fluid out of the pump. The positive pressure was increased from 55 to 110 kPa. A stable pumping capacity was found to be approximately 1.3 μL/stroke for the 5.3 mm diaphragm.

As expected, pumping capacity is related to the deflection level of the diaphragm. At negative pressures of -14 kPa or higher, no pumped flow occurred. At -17 kPa,

while no self-priming was observed, pumping capacity was measured to be 0.48 μL/stroke after forced priming. A linear zone was observed and pumping capacity increased from 0.64 to 1.64 μL/stroke when the negative pressure was decreased from -21 to -83 kPa. This demonstrates a decent operation zone within the elastic region of the PS material we used.

The effect of backpressure on pump capacity was also evaluated using a pump with a diaphragm of 5.3 mm in diameter. At backpressures less than 69 kPa, the pumping capacity remained constant at around 1.43 μL/stroke. When the backpressure was greater than 76 kPa, however, the pumping capacity starts to rapidly decline, reaching 0.22 μL/stroke at a backpressure of 90 kPa. At backpressures greater than 90 kPa, the pumping rate becomes negligible. Fortunately, most on-chip pumping applications utilize much lower backpressures (e.g., less than 41 kPa).

3.2.4 Pumping rate and pumping capacity: a function of pumping frequency

The effect of pumping frequency on pump rate and capacity was evaluated using a pump with a diaphragm of 5.3 mm in diameter and maintaining positive and negative pressures of 60 kPa and –55 kPa, respectively for pump actuation. Pumping frequency is defined as the number of pumping cycles or strokes within one second. Therefore, the pumping rate is equal to pumping capacity time pumping frequency. Figure 6 shows the effect of pumping frequency. At frequencies less than 1.25, pumping capacity remains stable around 1.25 μL/stroke. As the frequency increases, the pumping capacity starts to decrease. Upon further increase in frequency above 10 Hz, the pumping capacity starts to rapidly drop to 0.1 μL/stroke. The pumping rate, however, demonstrates a different trend with nearly linear increase to the maximum of 8.5 μL/sec at 10 Hz. It starts to rapidly decrease as pumping capacity when frequency is greater than 10 Hz.

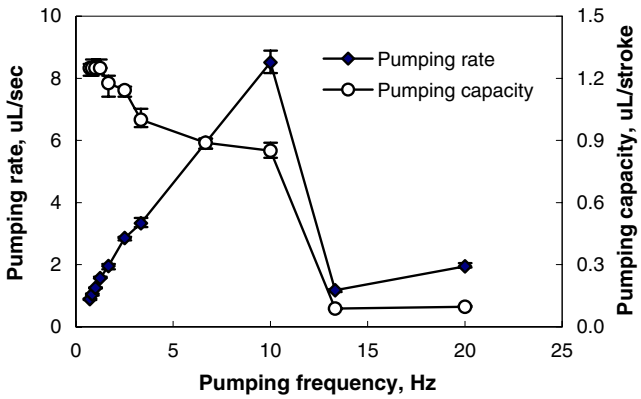

Fig. 6 Effect of pumping frequency on pumping rate and capacity

3.2.5 Reproducibility of pumping on different chips and effect of different fluids on pumping capacity

Five identical chips were tested using diaphragms of the same diameter of 5.3 mm. Identical sealing pressures of 69 kPa were applied to each pump while maintaining the negative pressures on all pumps at a consistent level of –55 kPa. The pumping capacities of the five individual chips were found to be consistent in the range of 1.44–1.50 μL/stroke, indicating exceptionally reproducible pump rates. Chips 1–4 were fabricated at the same time while chip 5 was fabricated 6 months later. Across the five chips, the standard deviation was observed to be 0.03 μL/stroke, which translates to a variation of 2% or a total of 1 μL per 34 strokes used to pump 50 μL of fluid, e.g., 2% variation.

In addition, preliminary tests were also performed using water containing popular reagents such as Triton X-100 and ethanol. With 1% Triton X-100 in water and 70% ethanol in water, pumping capacities were found to be 1.58, and 1.56 μL/stroke, respectively. This pumping capacity represents a 7% increase over that observed when just plain water was used, possibly due to improved wetting between triton- or ethanol-containing fluids and pump/channel surfaces.

4 Application examples and discussions

4.1 Valve sealing

In our design, a single diaphragm can serve as either an open/closed valve or as a pumping diaphragm. As a valve, the diaphragm can serve to open or close a particular conduit link within the microfluidic network or at the base of a particular reagent reservoir. Therefore, the requirements for valve sealing level depend on the specific application. At backpressures of 14, 28 and 41 kPa, the average leakage rates were found to be 0.003, 0.009 and 0.02 μL/min, respectively.

More challenging, however, is to use the diaphragm-based valves to seal a pressurized reactor (e.g., PCR, Fig. 7 (a)). Due to the various temperatures employed during PCR, especially the initial denaturation at approximately 95°C, the pressure build up within an integrated PCR chamber can be as high as 69 kPa. Fortunately, this pressure increase can be partially absorbed by the slight deflection of the plastic chamber itself. A pressure drop to 41–55 kPa provides an opportunity for us to use the diaphragm-based valves to seal the system.

4.2 Diaphragm-based agitation

Since most lab-on-a-chip applications require various mixing steps, we have demonstrated that when a cylindrical

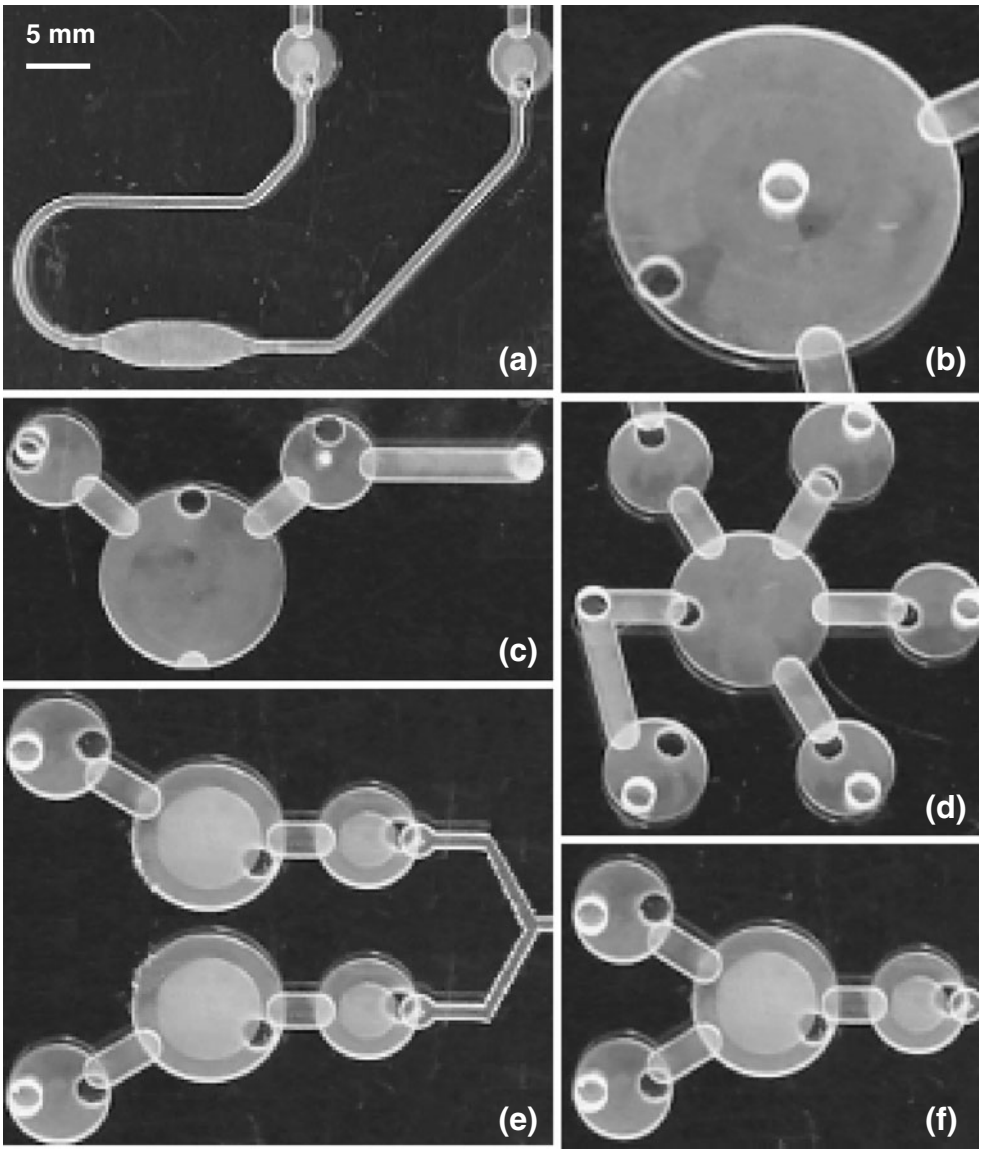

Fig. 7 Application examples. (**a**) Two valves used to seal inlet and outlet of a pressurized reactor. (**b**) Large diaphragm used to stir fluid inside reservoir attached above the center. (**c**) A single pump used for fluid transport between left and right ports. (**d**) Router function. (**e**) Two pumps used for simultaneous flow mixing. (**f**) Single pump for mixing by alternately opening left two valves

reservoir is attached above a large diaphragm pump, effective stirring can be achieved by simply pumping fluid in and out through the center orifice (Fig. 7(b)). This agitation scheme requires a relatively large pumping capacity of 4–8 μL/stroke, depending upon the volume of fluid to be mixed.

4.3 Fluid transport

Using our bi-directional diaphragm pumps, fluids can be easily transported from either side of the two valves linking the pumping diaphragm. As an example, Fig. 7(c) shows a pump consisting of one large pumping diaphragm and two small diaphragm valves. One port is shown directly on the left of the diaphragm while the other port is at the end of the conduit on the right. For this type of simple connection, minor leakage of a valve might not be a serious problem provided the pumping rate is maintained positively.

4.4 Router

Since many processes to be performed on a "lab-on-a-chip" require multiple reagents, the ability to accurately dispense and/or route two or more reagents may be necessitated by the particular application. Because our chip can be configured to achieve complex routing, such capabilities are readily possible. For example, Fig. 7(d) displays a chip with four valves linked to a center diaphragm and then joining to a separate valve. By selective opening and closing of these various valves and center diaphragm, complex fluidic routing functions can be achieved.

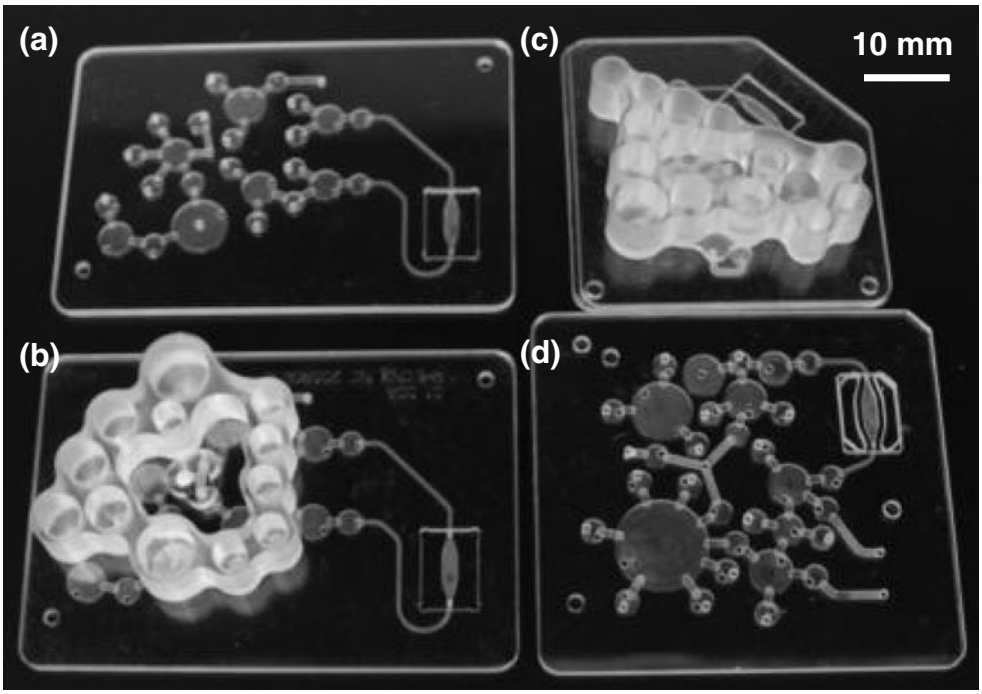

Fig. 8 Images of our various integrated chips. (**a**) integrated nucleic acid purification and PCR chip; (**b**) a reservoir panel attached to a); (**c**) modified version of b); and (**d**) chip integrating with sample introduction, nucleic acid purification, PCR and later flow detection (reservoir panel and detection strips not attached)

4.5 Pumping based mixing

We have practiced three different pumping-based mixing schemes. The first is to use a single pump to circulate fluids between two reservoirs by using several rounds of bi-directional flow (see the video entitled "Circulation Pumping" in the Supplementary Material). The second approach is based upon alternately opening the two inlet valves that share a single pumping diaphragm (Fig. 7(f)). Mixing is accomplished by splitting fluids into small slugs and flowing in an alternate sequence (i.e., fluid A-fluid B-fluid A-fluid B…). The third pumping method uses two separate pumps to simultaneously inject two fluids into either a common conduit (Fig. 7(e)) or a common outlet valve. The pumping diaphragm recovers from full deflection to flat status within 50 ms, resulting in average flow velocities of tens even hundreds mm/sec at the outlet hole or conduits. This results in a fairly high Reynolds number

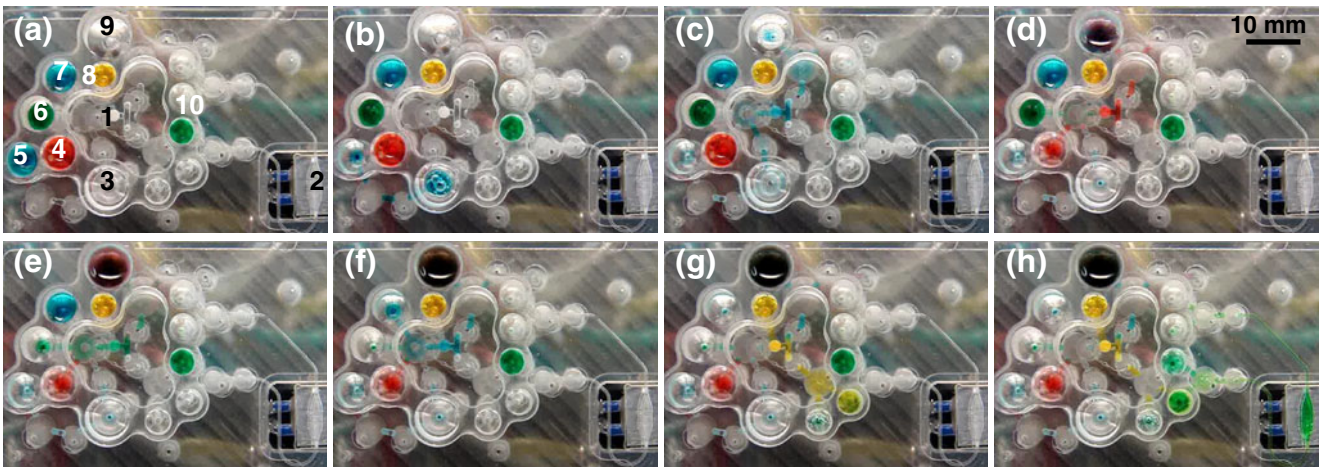

Fig. 9 Flow control demonstration of an integrated nucleic acid purification and PCR chip with dyed water. (**a**) description of chip: 1- silica membrane, 2-PCR chamber, 3-reservoir for sample loading and mixing, 4-ethanol, 5-lysis buffer, 6-wash buffer1, 7-wash buffer2, 8-elution buffer, 9-reservoir for waste, 10-PCR master mix; (**b**) lysis buffer pumped to mixer; (**c**) lysate pumped through silica membrane to waste; (**d-f**) ethanol, wash buffer1 and wash buffer2 sequentially pumped to wash silica membrane followed by vacuum drying of the silica membrane; (**g**) elution buffer pumped through silica membrane; and (**h**) eluted nucleic acid mixed with PCR master mix and pumped into PCR chamber

to cause chaotic flow, securing a fast and effective mixing process (see the video entitled "Dual Pump Mixing" in the Supplementary Material).

4.6 Integrated chips

Shown in Fig. 8 are some examples of various versions of the integrated chips, demonstrating the excellent bonding quality achieved by our weak solvent lamination process. Utilizing various configurations of on-chip valves and pumps, the fully automated flow control of an integrated chip for sample lysis, nucleic acid purification and PCR is demonstrated. Figure 9 is time lapse photography of the flow control demonstrated with dyed water (see the video entitled "Flow control of integrated chip" in the Supplementary Material). We have produced several hundreds of such chips. These chips were designed for sample lysis, nucleic acid extraction, and PCR amplification. Extensive tests on such chips have been conducted internally and externally (New York Univ., Lehigh Univ., Cornell Univ. and Leiden University of the Netherlands) achieving excellent purification and amplification of DNA/RNA, with results comparable to those obtained using manual "bench top" methods (data will be shown in a separate paper). The present technology and chip have been heavily evaluated for rapid biomedical diagnosis of HPV, HIV, etc., and they are currently in the process of commercialization.

5 Conclusions

We have described a design and fabrication method for a microfluidic device which differentiates itself from other well known art in the field with respect to the following aspects: polystyrene, a thermoplastic, is used as fabrication material; the device is weak-solvent laminated under mild conditions without damage to the underlying microfeatures; and all active control components, such as valves and pumps, are fabricated on-chip in a 3-layer structure, leading to a completely embedded fluidic network. Systematic characterization of the valve and pump has been presented. Not only is the sealing capacity of valve acceptable for various types of fluidic operations, but the pump also can be used for fluidic transfer, metering and mixing. Based upon the extremely low material costs, simple fabrication processes, and reliance upon existing industrial infrastructure for production of injection molded parts, we believe that our approach provides an opportunity to realize the promise of "lab-on-a-chip" technology and manufacture highly functional microfluidic devices at an affordable cost using high throughput, scalable production methods.

Acknowledgements We wish to thank Dr. Richard Montagna for his editorial assistance and helpful discussions. The Rheonix engineering group is gratefully acknowledged for its support in all aspects of chip fabrication.

References

A. Baldi, Y.D. Gu, P.E. Loftness, R.A. Siegel, B. Ziaie, J Microelectromech Syst **12**, 613 (2003)
H.H. Bau, J. Zhu, S. Qian, Y. Xiang, Sensor Actuator B **88**, 205 (2003)
L. Brown, T. Koerner, J.H. Horton, R.D. Oleschuk, Lab Chip **6**, 66 (2006)
D.J. Beebe, J.S. Moore, J.M. Bauer, Q. Yu, R.H. Liu, C. Devadoss, B. H. Jo, Nature **404**, 588 (2000)
A. Brask, J.P. Kutter, H. Bruus, Lab Chip **5**, 730 (2005)
K.K. Chee, Malaysian J Chem **7**, 57 (2005)
Z. Chen, M.G. Mauk, J. Wang, W.R. Abrams, P. Corstjens, R.S. Niedbala, D. Malamud, H.H. Bau, Ann. NY Acad. Sci. **1098**, 429 (2007)
Z. Chen, J. Wang, S. Qian, H.H. Bau, Lab Chip **5**, 1277 (2005)
J.S. Go, S. Shoji, Sensor Actuator A **114**, 438 (2004)
D.W. Green, R.H. Perry, *Perry's chemical engineers' handbook*, 8th edn. (McGraw-Hill, New York, 2008)
W.H. Grover, A.M. Skelley, C.N. Liu, E.T. Lagally, R.A. Mathies, Sensor Actuator B **89**, 315 (2003)
W. Gu, H. Chen, Y.C. Tung, J.C. Meiners, S. Takayama, Applied Physics Letters **90**, 033505 (2007)
A. Hatch, E. Kamholz, G. Holman, P. Yager, K. Bohringer, J Microelectromech Syst **10**, 215 (2001)
Y. He, Y.H. Zhang, E.S. Yeung, J. Chromatogr. A **924**, 271 (2001)
H.B. Hopfenberg, L. Nicolais, E. Drioli, Polymer **17**, 195 (1976)
Z. Hua, R. Pal, O. Srivannavit, M.A. Burns, E. Gulari, Lab Chip **8**, 488 (2008)
V. Lemoff, A.P. Lee, Sensor Actuator B **63**, 178 (2000)
R.H. Liu, J. Yang, R. Lenigk, J. Bonanno, P. Grodzinski, Anal. Chem. **76**, 1824 (2004a)
R.H. Liu, J. Bonanno, J.N. Yang, R. Lenigk, P. Grodzinski, Sensor Actuator B **98**, 328 (2004b)
Q. Luo, S. Mutlu, Y.B. Gianchandani, F. Svec, J.M.J. Fréchet, Electrophoresis **24**, 3694 (2003)
D.A. Mair, M. Rolandi, M. Snauko, R. Noroski, F. Svec, J.M.J. Fréchet, Anal. Chem. **79**, 5097 (2007)
L. Martynova, L.E. Locascio, M. Gaitan, G.W. Kramer, R.G. Christensen, W.A. MacCrehan, Anal. Chem. **69**, 4783 (1997)
J.C. McDonald, D.C. Duffy, J.R. Anderson, D.T. Chiu, H. Wu, O.J. Schueller, G.M. Whitesides, Electrophoresis **21**, 27 (2000)
S.H. Ng, R.T. Tjeung, Z.F. Wang, A.C.W. Lu, I. Rodriguez, N.F. de Rooij, Microsyst. Technol. **14**, 753 (2008)
R. Pal, M. Yang, B.N. Johnson, D.T. Burke, M.A. Burns, Anal. Chem. **76**, 3740 (2004)
J. Pipper, M. Inoue, L.F. Ng, P. Neuzil, Y. Zhang, L. Novak, Nat. Med. **13**, 1259 (2007)
J.J. Shah, J. Geist, L.E. Locascio, M. Gaitan, M.V. Rao, W.N. Vreeland, Anal. Chem. **78**, 3348 (2006)
H. Shinohara, T. Suzuki, F. Kitagawa, J. Mizuno, K. Otsuka, S. Shoji, Sensor Actuator B **132**, 368 (2008)
J. Steigert, S. Haeberle, T. Brenner, C. Müller, C.P. Steinert, P. Koltay, N. Gottschlich, H. Reinecke, J. Rühe, R. Zengerle, J. Ducrée, J. Micromech. Microeng. **17**, 333 (2007)
C.W. Tsao, L. Hromada, J. Liu, P. Kumar, D.L. DeVoe, Lab Chip **7**, 499 (2007)
M.A. Unger, H.P. Chou, T. Thorsen, A. Scherer, S.R. Quake, Science **288**, 113 (2000)

T.I. Wallow, A.M. Morales, B.A. Simmons, M.C. Hunter, K.L. Krafcik, L.A. Domeier, S.M. Sickafoose, K.D. Patel, A. Gardea, Lab Chip **7**, 1825 (2007)
J. Wang, Z. Chen, M.G. Mauk, K. Hong, M. Li, S. Yang, H.H. Bau, Biomed. Microdevices **7**, 313 (2005)
G.M. Whitesides, Nature **442**, 368 (2006)
P. Yager, T. Edwards, E. Fu, K. Helton, K. Nelson, M.R. Tam, B.H. Weigl, Nature **442**, 413 (2006)
L.C. Young, P. Zhou, United States Patent Application 20060076068, April 13, 2006.
S. Zeng, C.H. Chen, J.C. Mikkelsen, J.G. Santiago, Sensor Actuator B **79**, 107 (2001)
P. Zhou, L.C. Young, United States Patent 7,608,160, October 27, 2009.
Z. Zou, J. Kai, M.J. Rust, J. Han, C.H. Ahn, Sensor Actuator A **136**, 518 (2007)